The entrainment due to a turbulent fountain at a density interface

By Y. J. P. LIN† AND P. F. LINDEN

Department of Mechanical and Aerospace Engineering, University of California, San Diego,
9500 Gilman Drive La Jolla, CA 92093-0411, USA

We describe new experiments to measure the penetrative entrainment by a turbulent fountain in a steady two-layer stratification. A theoretical model was established by assuming that the stratification consists of two uniform layers, and the penetrative entrainment rate is estimated quantitatively by three independent formulae. Two quasi-uniform layers were observed in the steady state in the laboratory experiments. Experimental results gave a nearly constant penetrative dimensionless entrainment rate (0.65 ± 0.17) across a density interface when the local Richardson number is smaller than 1.2.

1. Introduction

The aim of this study is to investigate penetrative entrainment by a turbulent fountain at a density interface of a two-layer fluid. Penetrative entrainment plays a crucial role in determining the stratification in a space ventilated with an Under Floor Air Distribution system (hereinafter referred to as UFAD), which is an emerging cooling strategy for commercial buildings. In a UFAD system, cool air is blown upwards into a space. This cool dense air is driven upwards by the momentum flux of the air which is usually imparted by a pressure difference between an underfloor plenum and the air in the room. Under normal operating conditions, this cool air forms a turbulent 'fountain' (Turner 1966), which entrains air from its surroundings as it rises. In most UFAD applications, warm air produced by heat sources is extracted at the ceiling and the fountain impinges on this warmer upper region. Since the fountain is relatively cold, it falls down after reaching some height and entrains and transports downwards some of this warm air. This paper provides a measure of this entrainment. See Webster, Bauman & Reese (2002), Bauman (2003) and Lin & Linden (2005) for details of the performance of this cooling system.

Penetrative entrainment by a turbulent fountain is also used to recirculate a water reservoir, such as a pond or a lake, and can have a significant effect on water quality. Usually, stable stratification suppresses the vertical exchange of water masses and results in stagnation zones with inferior water quality. Momentum water jets aid the vertical water mass transport and prevent the establishment of stable density stratification (Stephens & Imberger 1993; Larson & Jonsson 1996).

† Present address: Energy & Resources Lab., Industrial Technology Research Institute, Bldg 64, 195, Sec. 4, Chung Hsing Road, Chutung, Hsinchu, Taiwan 310.

1.1. *A turbulent fountain*

Different signs (positive, zero and negative) of buoyancy from a jet source categorize three different jet structures as a buoyant jet, a pure jet and a fountain (or a negatively buoyant jet), respectively. In this study, we focus on the structure of a fountain. A fountain occurs when the initial momentum is upward and the jet fluid is negatively buoyant (or vice versa). The (negative) buoyancy force decreases the momentum flux in the jet with height. At some height the momentum flux is zero, and the flow then reverses and falls down around the core upward flowing jet.

A fountain has a similar dynamical structure to that of a pure jet before reversing its direction of motion. The reversal of the flow direction changes several dynamical properties of a fountain. For example, the maximum height a fountain is able to reach decreases after it reverses. When the jet is initially turned on, the jet fluid entrains the stationary ambient fluid and reaches an initial maximum height z_i. Because the fluid is denser than the surrounding fluid, once it loses its upward momentum it falls down around the jet in an annular region adjoining the upward flow. Since the outer-layer fluid of oppositely directed momentum reduces the inner-layer upward momentum more than the stationary ambient fluid before the inversion takes place, the final maximum height z_m shrinks after this reversal happens and other properties, such as velocity and buoyancy in the fountain, change too. The two different maximum distances, z_i and z_m, have been measured and the ratio of z_i/z_m has a mean value 1.43, as reported in Turner (1966).

On the basis of dimensional analysis, Turner (1966) proposed that the final maximum height z_m in a uniform density environment is

$$z_m = C_f M_0^{3/4}|F_0|^{-1/2}, \tag{1.1}$$

where C_f is a dimensionless constant determined from experiments, M_0 is the initial momentum flux and F_0 is the initial buoyancy flux of the fountain source. The experimentally determined constant value C_f is observed to vary from 1.70 to 1.85 (Turner 1966; Mizushina *et al.* 1982; Baines *et al.* 1990; Bloomfield & Kerr 2000) under different source conditions.

The solutions of the governing equations of plume motion have been successfully used to predict the initial height a turbulent fountain reaches before the downflow has formed (Morton 1959; Bloomfield & Kerr 1998). However, these equations can no longer be applied once the downflow begins to interact with the upflow. To overcome this problem, Turner (1966) proposed that it should be possible to set up a detailed theory of the 'double' structure of the fountain in the manner suggested by Morton (1962) for coaxial turbulent jets.

The ideas presented in Morton (1962) on the rate of entrainment between two turbulent flows were subsequently used by McDougall (1981) to develop a theoretical model of an axisymmetric fountain in a homogeneous fluid. This model was based on a set of new entrainment equations which quantified the mixing between the upflow and the downflow, and between the downflow and the environment. In addition to the effects of mixing between the flows, McDougall (1981) also recognized that the body forces acting on the fluid in the upflow and downflow are 'very much an open question'. In an attempt to address this question, McDougall (1981) considered the two most reasonable formulations of the body forces acting on the fountain, and was able to predict the final fountain height as well as the width, velocity and buoyancy in the upflow and downflow. In that investigation, only the predictions of the fountain

height were compared with experimental data, since measurements of the internal fountain structure did not become available until the study by Mizushina *et al.* (1982).

Bloomfield & Kerr (2000) presented a new model of a turbulent fountain which is based on the ideas developed by McDougall (1981), but in which they considered an alternative formulation for the entrainment between the upflow and the downflow. The set of entrainment equations implementing their entrainment formulation results in a good prediction on the initial height and a closer prediction to the value of the final height than the previous theoretical models. We will use the model of Bloomfield & Kerr (2000) in numerical calculations to estimate the properties of a turbulent fountain in this study.

1.2. *Penetrative entrainment across an interface*

Penetrative entrainment is often encountered in nature. Turner (1968) carried out pioneering experiments on entrainment across a density interface. In these experiments, the turbulence was generated by oscillating grids located parallel to and at some distance from the interface. The turbulence generated by the grid decays with distance from the grid, and Turner made the important conceptual leap of describing the entrainment in terms, of local variables determined at the position of the interface. He reasoned that the entrainment would depend on the buoyancy step $\Delta g' = g\Delta\rho/\rho$ across the interface and, on the turbulence intensity w and length scale l at the interface. He presented his measurements in terms of a dimensionless entrainment rate $E = u_e/w$ where u_e is the measured entrainment velocity, and argued that $E = E(Ri)$ where Ri is the local Richardson number at the interface defined by

$$Ri = \frac{\Delta g' l}{w^2}. \tag{1.2}$$

For our purposes, it is more convenient to define E in terms of volume fluxes, so that the entrained volume flux Q_E is given by

$$Q_E = E(Ri)Q_{int}, \tag{1.3}$$

where Q_{int} is a measure of the turbulence volume flux at the interface, which will be defined precisely below. Generally, entrainment is reduced as the stability of the interface increases, so we expect E to be a decreasing function of Ri. Linden (1973), from a study of the interaction of a vertically propagating vortex ring on an interface, found $E \propto Ri^{-3/2}$, in agreement with the experimental results of Turner (1968) for a high-Péclet-number interface.

Work on the penetrative entrainment across a density interface by discrete flow structures has considered the impingement by a vortex ring (Linden 1973), impingement by a buoyant plume (Baines 1975; Kumagai 1984; Cardoso & Woods 1993) and entrainment by a turbulent jet (Larson & Jonsson 1994, 1996; Shy 1995). In this paper, some of studies on penetrative entrainment by a buoyant plume are reviewed and applied since similar dynamic behaviours occur in both the buoyant plume and the fountain.

Baines (1975) studied a plume or jet impinging on a density interface and showed that the entrainment rate E was also proportional to $Ri^{-3/2}$, where

$$Ri = \frac{\Delta g' b_{int}}{w_{int}^2}, \tag{1.4}$$

where w_{int} and b_{int} are, respectively, the vertical velocity and the radius of the buoyant plume at the density interface position. Baines (1975) used the Froude number rather

than the Richardson number to analyse his experimental data, but two parameters are interchanged as ($Fr = Ri^{-1/2}$). Using the Gaussian distribution of velocity and radius profiles, he presented the experimental results of $0.4 < Fr < 2.4$, which correspond to $1 < Ri < 36$ for the top-hat distribution which is applied in this paper.

Kumagai (1984) studied the same problem, but extended the range of Ri to $0.1 < Ri < 70$. He gave an empirical formula for the penetrative entrainment rate to fit his experimental results (cf. equation (4.5) in his paper) for this range of values of Ri,

$$E = \frac{Ri^{-3/2}}{1 + 3.1 Ri^{-1} + 1.8 Ri^{-3/2}}. \tag{1.5}$$

When Ri is much larger than unity, the entrainment rate is proportional to $Ri^{-3/2}$, as found by Baines (1975). As Ri decreases, the penetrative entrainment rate tends to approach a constant value. The limit $Ri \to 0$ of (1.5) gives a constant value of 0.56, but the experimental results of Kumagai (1984) appear to be closer to a constant of 0.32 when $Ri \to 0.1$. The values given by (1.5) in the limit $Ri \to 0$ may not be reliable.

Cardoso & Woods (1993) proposed that the mixing at a density interface by a turbulent plume was proportional to Ri^{-1}, rather than $Ri^{-3/2}$, over an intermediate range of Ri, $1.2 < Ri < 25$. This model gave a better fit to the results of Kumagai (1984) over this range of Ri.

In a related study, Larson & Jonsson (1994, 1996) carried out experiments on the destratification of a two-layer stably stratified fluid by a turbulent water jet. A jet was discharged vertically downwards in a confined fluid system consisting initially of a top layer of fresh water and a bottom layer of salt water. They measured the percentage of the supply kinetic jet energy used for increasing the potential energy of the fluid system, in order to determine the mixing efficiency in several different environmental conditions, where the diameter and exit velocity of the jet were varied together with the density difference between the top and bottom layers. In contrast to the other studies referenced above, Larson & Jonsson (1994, 1996) used the kinetic energy at the exit of a momentum jet as the available kinetic energy to calculate the mixing efficiency rather than the kinetic energy at the density interface. It is, therefore, difficult to relate their results to the previous work on buoyant plumes.

The penetrative entrainment by a turbulent fountain is similar to that by a jet or plume. On the basis of a similarity between the two flows, the local Richardson number in the turbulent fountain at the density interface is assumed to determine the penetrative entrainment of a fountain.

In this study, we describe a new experimental arrangement to maintain a steady two-layer stratification and present measurements of the penetrative entrainment between the density interface due to a turbulent fountain in the steady state. We restrict attention to flows where $Ri < 1.2$, which is a parameter range of relevance to the operation of UFAD systems. The format of this paper is as follows. Section 2 proposes an arrangement for penetrative entrainment measurements, then describes the flow qualitatively and presents a physical model for the flow. Section 3 describes the laboratory experiments, techniques to investigate the flow and the experimental conditions. Section 4 presents experimental results of steady state and estimates of penetrative entrainment. Section 5 gives some discussion on characteristics of the flow, the plume theory and the fountain model used in this study. Finally, § 6 draws some conclusions and discusses some applications of this study.

2. Penetrative entrainment measurements

2.1. *Arrangement*

Certain conditions are necessary for maintaining a steady state in an environment in a non-diffusive fluid. For an incompressible fluid without sources and sinks of mass, conservation of mass is

$$\frac{D\rho_e}{Dt} = 0, \tag{2.1}$$

where ρ_e is the environmental density. In a stably stratified fluid, horizontal density variations are observed to be small compared with vertical variations, since a small horizontal difference in the density distribution produces horizontal flow that tends to homogenize the density distribution at the same elevation. Consequently, except in isolated regions of high convective activity, such as in a plume or jet, the density distribution in the steady state ρ_e is a function of the vertical variable z only

$$\rho_e = \rho_e(z). \tag{2.2}$$

Then, in a steady state, (2.1) can be rewritten as

$$w\frac{\partial \rho_e}{\partial z} = 0. \tag{2.3}$$

Thus, the conditions required to maintain a steady state are either zero vertical velocity $w = 0$ or zero density gradient $\partial \rho_e/\partial z = 0$ in a space. The space maintaining steady-state stratification has regions with vertical flow and uniform density, or stratified regions with no vertical motion. Generally, there are individual layers, each with uniform density in which there is vertical motion, separated by density interfaces at which there are no vertical motion.

In order to maintain a steady two-layer stratification in which we could measure the entrainment, a dense plume source was used to produce a heavy layer at the bottom of a tank. The turbulent fountain was produced as a momentum jet with downward momentum, emitted from a source positioned at the same depth as the plume source as sketched in figure 1. A siphon pipe withdrew the fluid from near the free surface to keep a constant volume of fluid in the tank. The fountain source is supplied with the fluid of the density ρ_f.

In this arrangement, there are two constant continuous injection sources in the space. Two-layer stratification is observed in the steady state, with $w = 0$ but $\partial \rho_e/\partial z \neq 0$ at the density interface. The fluids of the two layers in the environment do not penetrate the interface except in the plume and fountain where (2.3) is invalid.

In the upper and lower layers, $\partial \rho_e/\partial z = 0$ and $w \neq 0$ since the fluid is driven by the supplies from the plume and the fountain. The fluid motion in the environment outside the plume and the fountain is upward in both layers. The supply from the plume arrives at the bottom of the tank and then lifts the existing fluid upward. The fluid in the lower layer is entrained by the fountain across the density interface. The fluid in the fountain supplies the upper layer from the base. The system achieves a steady two-layer stratification when the volume flux in the plume and the entrained volume flux by the fountain at the density interface balance each other. Thus, this arrangement provides a direct measure of the penetrative entrainment. It is also necessary for the buoyancy fluxes in the two layers to balance in the steady state. As will be shown in §2.3, this condition provides an alternative way of calculating the penetrative entrainment.
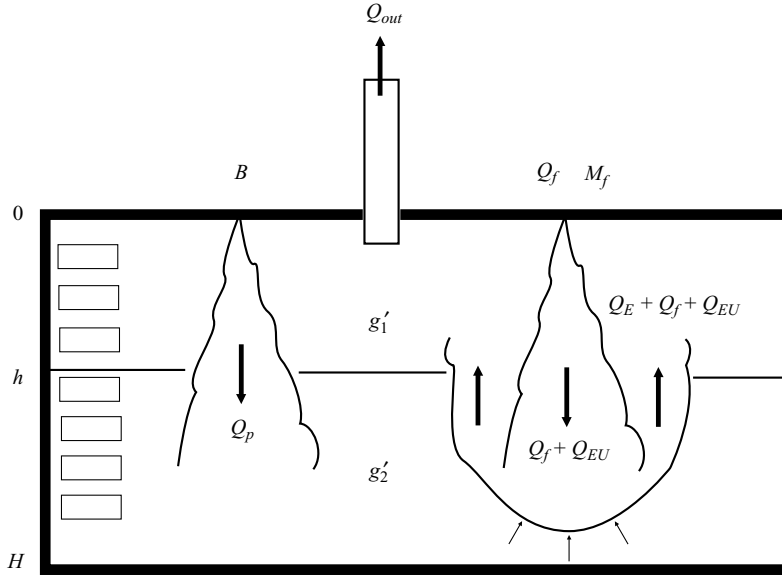
FIGURE 1. A sketch of the experimental arrangement for determining the penetrative entrained volume flux Q_E due to a momentum jet (fountain) at a density interface in the steady state. A dense plume is on the left-hand side, a downward fountain is on the right-hand side and a siphon pipe entrance is positioned at the free surface to withdraw fluid in the tank. The figure also shows a schematic of the positions of lighting intensity windows on the tank.

2.2. *Description of the flow*

Before presenting the theoretical model and the detailed experimental results, the laboratory experiment and the physical ideas are described in qualitative terms. The basis for the quantitative model will then become clear.

As the plume and the fountain are turned on, the plume fluid (salt solution) arrives at the bottom of the tank and forms a dense layer in an initially fresh-water environment.† The fountain arrives at the interface, at the top of this dense layer, then penetrates into it for some distance, and rises back to the upper layer since it is less dense than the lower layer. The process of the fountain penetrating into the dense layer brings a certain volume of the fluid in this layer to the upper layer. This penetrative entrained fluid, mixed with the fluid in the fountain, rises and modifies the properties of the upper layer.

A series of transient flow images, from Experiment 5 (which will be described in §3), obtained at 2, 8, 14 and 20 min, respectively, after turning on the plume and fountain sources are shown in figure 2. At the beginning of the experiment, the plume supplies the lowest density fluid to the lower layer since the ambient fresh-water environment, which is entrained into the plume, has the smallest density at this time. The turbulent fountain also propagates the furthest vertical distance in the fresh-water environment initially, since there is the smallest negative buoyancy force.

---

† In our experiments, the density of the fountain supply fluid is the same as that initially in the tank (they are both fresh water). However, this condition is not necessary. If the fountain source has an initially different density, the same steady state is achieved, but it is first necessary to replenish the fluid in the tank with the fountain fluid.
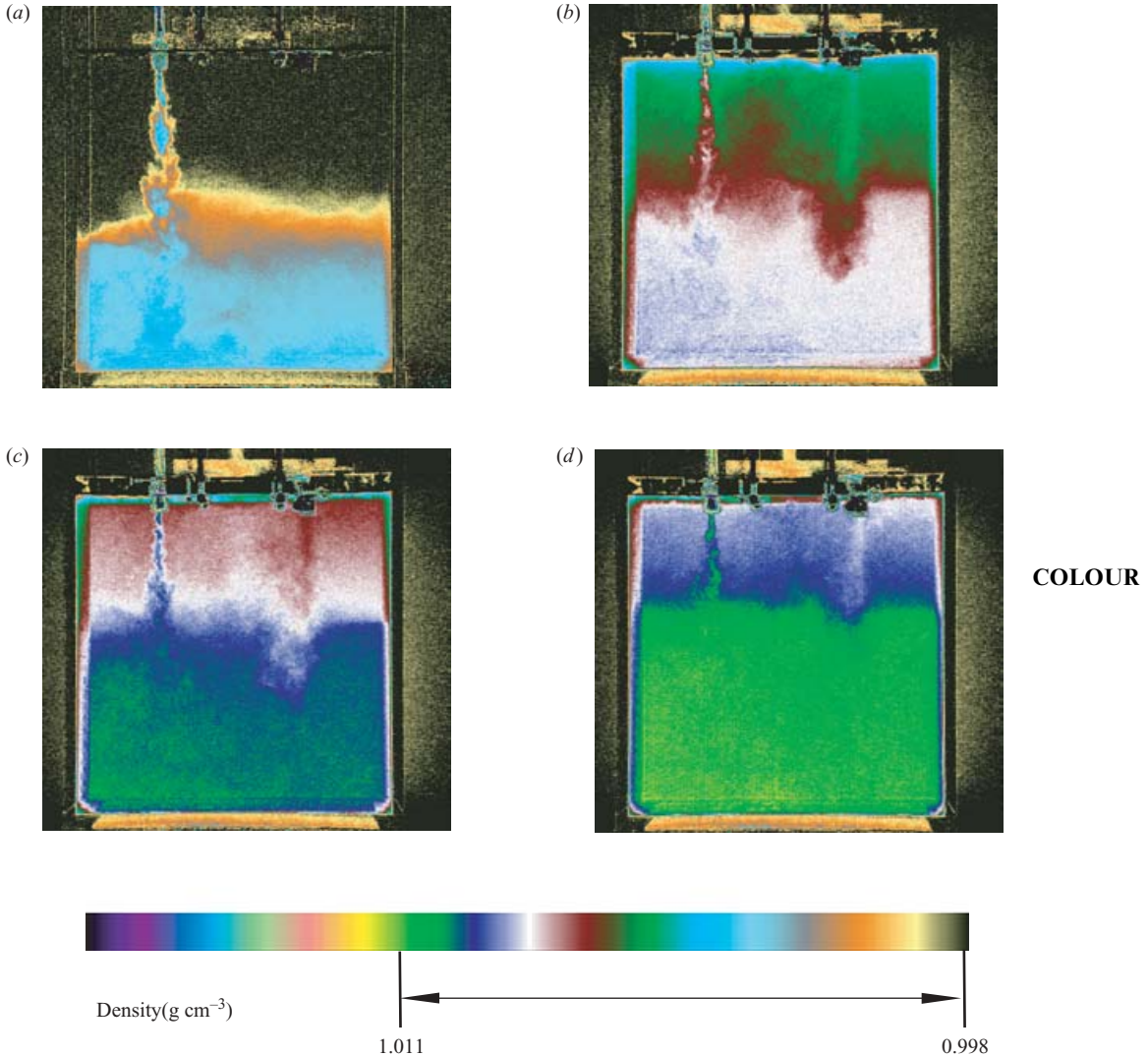
(a)

(b)

(c)

(d)

COLOUR

Density(g cm^{-3})

1.011

0.998

FIGURE 2. Four transient images were taken from Experiment 5. There is a 6 min interval between each two consecutive images. (*a*), (*b*), (*c*), (*d*) were taken at 2, 8, 14 and 20 min, respectively, after the plume and the fountain sources are switched on. All images were corrected for variations in the background lighting.

The penetration into and subsequent rise from the heavy lower layer of the turbulent fountain entrains some of the fluid into the upper layer. The density of the upper layer is modified (increased) by this penetrative entrained fluid. As the density of the upper layer increases, the downward momentum of the fountain is reduced more quickly by the buoyancy force and so the fountain penetrates a shorter distance into the lower layer. As a result, the interface moves upward and the densities in both the layers increase with time until steady state is reached.

When the volume fluxes and buoyancy fluxes balance between two layers and in the space, a steady two-layer stratification is maintained. Figure 3(*a*) shows an image of the steady-state flow which was taken at 120 min after turning on the plume
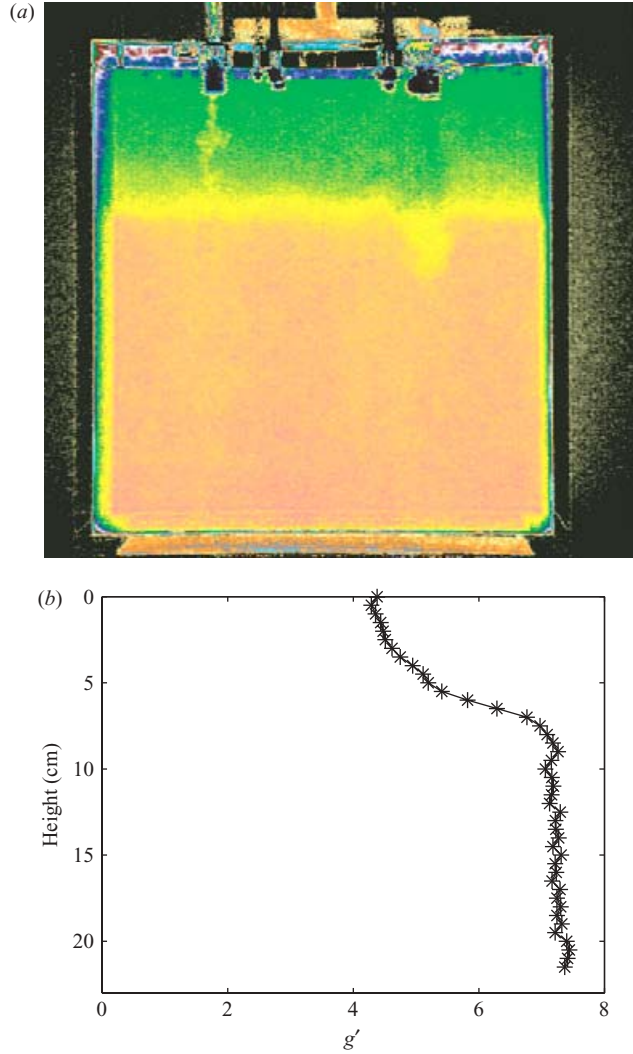
FIGURE 3. (*a*) An image taken from Experiment 5 in tank 2, after the experiment had run for 120 min. The image was corrected for variations in the background lighting. The plume is on the left-hand side and the fountain is on the right-hand side, and we can see the two layers produced by them. (*b*) The corresponding reduced gravity profile of the steady-state flow. There are two different layers established in the tank. The lower layer is well mixed, but the upper layer retains some weak vertical stratification.

and fountain sources in Experiment 5. Figure 3(*b*) shows the corresponding reduced gravity profile, and an approximate two-layer stratification is observed in this figure. The lower layer is well mixed, but the upper layer retains some weak stratification. In the following section, a theoretical steady-state two-layer model will be discussed.

2.3. *Theoretical model*

In the steady state, the buoyancy input in the space balances the buoyancy extracted, as shown in figure 1, i.e.

$$B = g'_1 Q_{out}, \tag{2.4}$$

where B is the buoyancy flux of the plume, and Q_{out} is the volume rate extracted from the tank. The reduced gravity of the upper layer is g_1'

$$g_1' = \frac{\rho_1 - \rho_f}{\rho_f} g, \qquad (2.5)$$

where ρ_1 is the density of the upper layer, ρ_f is the density of the fluid from the fountain source and is used as the reference density, and g is the acceleration due to gravity. The choice of ρ_f as the reference density implies that the fountain introduces no buoyancy ($g_f' = 0$). Provided the Boussinesq approximation is valid $\Delta\rho \; (= \rho_1 - \rho_f) \ll \rho_f$, the choice of the reference density is unimportant. In the laboratory experiments, the buoyancy flux is produced by a small volume flux Q_s of dense fluid. The buoyancy flux is $B = g_s' Q_s$ where g_s' is the reduced gravity of the salt solution supplying the plume source.

Volume conservation in the space is

$$Q_{out} = Q_f + Q_s, \qquad (2.6)$$

where Q_f is the volume flux from the fountain source. Since $Q_s \ll Q_f$ in these experiments, we approximate it by assuming

$$Q_{out} \approx Q_f, \qquad (2.7)$$

so hereinafter Q_f is used instead of Q_{out}.

Volume conservation of the lower layer is

$$Q_p = Q_E, \qquad (2.8)$$

where Q_p is the volume flux of the plume at the interface and Q_E is the penetrative entrained volume flux from the lower layer to the upper layer by the fountain. As discussed above, because the volume exchange between two layers occurs only in the plume and the fountain regions, these two quantities have to balance in the steady state.

The entrainment flux Q_E can be determined in terms of the plume properties by applying the plume theory of Morton, Taylor & Turner (1956). This gives the volume flux as

$$Q_p = Q_p(h, B_r) = C B_r^{1/3} h^{5/3}, \qquad (2.9a)$$

and the reduced gravity difference between the two layers as

$$g_2' - g_1' = \Delta g'(h, B_r) = \frac{1}{C} B_r^{2/3} h^{-5/3}, \qquad (2.9b)$$

where g_2' is the reduced gravity of the lower layer

$$g_2' = \frac{\rho_2 - \rho_f}{\rho_f} g, \qquad (2.10)$$

h is the depth between the density interface and the origin of the plume, B_r is the buoyancy flux of the plume in the upper layer and C is the universal plume constant $C = 6\alpha/5(9\alpha/10)^{1/3}\pi^{2/3}$, where α is the entrainment constant of the plume. Here we use $\alpha = 0.083$ which is suggested by Turner (1986). Since, in steady state, the density of the upper layer is larger than the initial value, $B_r = (g_s' - g_1')Q_s$. The value of $g_s' \gg g_1'$, so B_r is only slightly smaller than B. Equations (2.9a) and (2.9b) show that the reduced gravity step between these two layers and the plume volume flux at the interface depend on the buoyancy flux of the plume and the distance between the plume source and the density interface.

The reduced gravity of the plume at the interface is the maximum value that can supply the lower layer, therefore it penetrates the interface, arrives and spreads out at the bottom of the tank and then lifts up the previously occupying fluid. When the flow reaches steady state, the plume introduces a constant maximum density fluid to the lower layer. Eventually, the density of the lower layer is equal to this supplying density and the previous fluid of lower density in this layer is removed from the top of the layer by penetrative entrainment of the turbulent fountain at the interface.

The reduced gravity of the fountain source g'_f is smaller than the reduced gravity of the upper layer g'_1 in the steady state, so the momentum of the fluid from the fountain source decreases owing to the buoyancy force as it propagates downwards. The residual momentum causes the fluid in the fountain to penetrate the density interface and then entrain a certain amount of the fluid from the lower layer to the upper layer. The fluid in the fountain reaching the interface consists of the source fluid Q_f plus the upper-layer fluid entrained into the fountain Q_{EU}. This fluid penetrates the lower layer for some distance before rising back up into the upper layer as a result of the buoyancy forces. As it does so, the fountain entrains lower-layer fluid with the reduced gravity g'_2 and brings it into the upper layer. The mixing of these three fluids of different properties determines the reduced gravity of the upper layer, i.e.

$$g'_1(Q_f + Q_{EU} + Q_E) = g'_f Q_f + g'_1 Q_{EU} + g'_2 Q_E. \tag{2.11a}$$

Since, by definition, the reduced gravity g'_f from the fountain source is zero, we simplify (2.11a) to obtain

$$g'_1 = \frac{g'_2 Q_E}{Q_f + Q_E}. \tag{2.11b}$$

Therefore, from the values of g'_1 and g'_2, both measured in the experiments, and a control parameter Q_f, the penetrative entrained volume flux Q_E can be determined from (2.11b) as

$$Q_E = \frac{g'_1 Q_f}{g'_2 - g'_1}. \tag{2.12}$$

The reduced gravity of the lower layer is determined by entrainment of the fluid from the upper layer into the plume and the buoyancy flux of the plume source, i.e.

$$g'_2 Q_p = B + g'_1(Q_p - Q_s). \tag{2.13}$$

Again, Q_s will be neglected in the analysis since $Q_s \ll Q_p$, so

$$g'_2 Q_p \approx B + g'_1 Q_p. \tag{2.14}$$

Using (2.4), (2.7) and (2.8), we have the left-hand side of (2.14) as

$$g'_2 Q_p = g'_2 Q_E, \tag{2.15}$$

and the right-hand side of (2.14) as

$$B + g'_1 Q_p = g'_1 Q_{out} + g'_1 Q_E = g'_1 Q_f + g'_1 Q_E = g'_1(Q_f + Q_E). \tag{2.16}$$

Therefore, (2.14) reproduces (2.11b).

Substitute (2.4) and (2.8) into (2.14) to obtain

$$g'_2 = B\left(\frac{1}{Q_p} + \frac{1}{Q_f}\right) = B\left(\frac{1}{Q_E} + \frac{1}{Q_f}\right). \tag{2.17}$$

Thus, the reduced gravity of the lower layer depends on the plume buoyancy flux, the source volume flux of the fountain and its entrained volume flux at the interface (or the supply volume flux from the plume at the density interface). It is noted that the volume flux from the fountain source has the same impact as the penetrative entrainment volume flux at the interface does on the reduced gravity of the lower layer.

The reduced gravity difference between the two layers $\Delta g'$ is estimated by (2.4) and (2.17), i.e.

$$\Delta g' = g'_2 - g'_1 = \frac{B}{Q_E} = \frac{B}{Q_p}, \qquad (2.18)$$

since $Q_p = Q_E$, see (2.8). This reduced gravity step only depends on the buoyancy flux of the plume and the penetrative entrainment volume flux at the interface.

Therefore, there are three different formulae to estimate the value of the penetrative entrained volume flux Q_E. These are:

(*a*) the penetrative entrained volume flux equal to the supply volume flux in the plume at the density interface (2.8) and the plume theory (2.9*a*); this estimate requires measuring the interface depth h and the buoyancy flux B_r of the plume relative to the upper layer in the steady state;

(*b*) the penetrative entrainment across the density interface by the fountain (2.12); this estimate requires measuring the reduced gravity g'_1, g'_2 of the two layers and the source volume flux Q_f of the fountain; and

(*c*) the mixing in the plume within the upper layer (2.18); this estimate requires measuring the density step $\Delta g'$ between the two layers and the buoyancy flux B from the plume.

In §4, the values of the penetrative entrained volume fluxes obtained from these three different measurements are presented and compared.

3. Laboratory experiments

Experiments were conducted in two different Plexiglas tanks: tank 1 was 28 cm wide, 58.5 cm long and filled with fresh water to a depth 25.0 cm; tank 2 was 15.0 cm wide, 30.0 cm long and filled with fresh water to a depth 23.0 cm. A plume source nozzle and a fountain source nozzle were both placed at the same elevation, 1 cm below the free surface. The coordinate position $z = 0$ was set at the height of the sources and z was positive downward as depicted in figure 1. A siphon pipe, 1.27 cm in diameter and connected to another constant-head tank, was placed in the Plexiglas tank to keep a constant volume of fluid in the tank. The end of the siphon pipe was positioned just below the free-surface level of the Plexiglas tank.

The plume nozzle is the same as that used in the experiments of Lin & Linden (2002), having 0.5 cm in diameter, and the details of the plume design can be found in Hunt & Linden (2001). The fountain nozzle, a straight tube 1.27 cm in diameter, is made of Plexiglas and its exit is attached with a piece of fine wire mesh (approximate aperture size 0.1 cm × 0.1 cm) to promote disturbance of the flow.

The density measurement technique, which was used in the experiments of Lin & Linden (2002), is based on the lighting intensity attenuation technique and the details of this technique are given in Cenedese & Dalziel (1998). Dye was added to the salt solution and the water from the fountain nozzle was undyed. The light attenuation due to the dye in the salt solution is related to the density of the solution. Before running experiments, we used the same lighting as in the experiments to record images

Run	B	Q_f	M_f	Running time (min)	Tank
1	83.97	13.8	200.44	90	1
2	85.73	21.7	495.64	100	1
3	48.60	13.8	200.44	100	1
4	48.60	21.7	495.64	100	1
5	83.07	13.8	200.44	360	2
6	83.07	21.7	495.64	120	2
7	45.07	13.8	200.44	300	2
8	45.07	21.7	495.64	110	2

TABLE 1. The 8 different experimental conditions. The buoyancy flux of the plume source B was varied by changing the concentration of salt solution, the volume flux of the fountain Q_f was measured by an inline flow meter and the momentum flux of the fountain M_f was estimated by (3.2). The running time of the experiment and the tank which was used are given in the table.

of sample solutions, and measured their densities with an Anton Paar density meter which has an accuracy of 2×10^{-6} g cm^{-3}. We used the light intensities of the sample solutions and their measured densities to interpolate the density distributions in the tank via experimental images. Experiments were recorded directly through a Cohu 4912 CCD camera into a microcomputer hard disk at 1 min intervals.

The dye intensity was measured in prescribed windows. The window size in tank 1 was 2 pixels high by 38 pixels wide (about 0.2 cm high by 5.5 cm wide), and in tank 2 was 2 pixels high by 30 pixels wide (about 0.1 cm high by 2.0 cm wide). The stratification in the tank environment was found to be generally horizontally uniform by comparing the lighting intensity at different horizontal locations at the same elevation outside both the plume and the fountain. In order to obtain vertical density profiles, a set of aligned windows was used. The positions of the windows used for measuring the lighting intensity in the tank are depicted schematically in figure 1. Each two adjacent windows have a 0.5 cm vertical interval between them. This measured density profile is believed to represent the stratification of the entire tank environment.

3.1. *Experimental conditions*

Salt solution was used as the plume supply fluid and fresh water as the fountain supply fluid. Different buoyancy fluxes B of the plume source, volume fluxes Q_f and momentum fluxes M_f of the fountain in 8 different experiments are given in table 1, along with the running time of the experiments and the tank used. The buoyancy flux of the plume source B was varied by changing the concentration of the salt solution, from 1.05 g cm^{-3} to 1.1 g cm^{-3}, and the plume source had a small fixed volume flux 0.9 cm^3 s^{-1} in all the experiments. The volume flux of the fountain Q_f was regulated by an inline flow meter. Note that $Q_s/Q_f < 0.07$, so the small source volume flux Q_s of the plume is negligible in the analysis. Nevertheless, when the data are analysed they are corrected for the non-zero values of Q_s.

The sources were positioned where the fountain and the plume did not interact with the sidewalls. The momentum fluxes M_f were controlled below 533.33 cm^4 s^{-2} since the turbulent fountain hit the bottom of the tank for larger values of M_f. The 8 experiments were chosen to represent two sets of similar parameters B, Q_f and M_f in two different tanks (see table 1).

A fixed cross-section area fountain source was used. We assumed the velocity profile $U(r)$ at the nozzle exit was parabolic and given by

$$U(r) = 2\frac{Q_f}{A}\left(1 - \frac{4r^2}{D^2}\right), \tag{3.1}$$

where $A = 1.27\,\text{cm}^2$ was the cross-section area, $\pi D^2/4$, and $D = 1.27\,\text{cm}$ was the diameter of the fountain nozzle source.

The momentum flux M_f was

$$M_f = \int_0^{D/2} 2\pi r U^2(r)\,\mathrm{d}r = \frac{4}{3}\frac{Q_f^2}{A}. \tag{3.2}$$

The Reynolds number at the fountain nozzle,

$$Re = \frac{w_0 D}{\nu}, \tag{3.3}$$

varied from 1380 to 2150 when the flow rate varied from $13.8\,\text{cm}^3\,\text{s}^{-1}$ to $21.7\,\text{cm}^3\,\text{s}^{-1}$. Here, $w_0 = Q_f/A$ is the mean exit velocity from the nozzle and ν is kinematic viscosity of water. The Reynolds number at the plume nozzle was 230 when the flow rate was fixed at $0.9\,\text{cm}^3\,\text{s}^{-1}$.

3.2. *The time of attaining steady state*

The time to attain steady state for the lower layer depends on the relative ratio of the lower-layer volume size and the penetrative entrained volume flux (which is equal to the volume flux supply from the plume to the lower layer in the steady state). The time of replacing the upper layer depends on the volume flux of the fountain source and the volume of the upper layer when a pure plume, without any volume flux from the source, is considered. Since the penetrative entrained volume flux across the density interface by the turbulent fountain is equal to the volume flux of the fluid in the upper layer entrained into the plume, the replacement of the upper layer is less efficient than that of the lower layer. A large portion of the fluid supplied from the fountain to the upper layer is entrained into the plume in this layer and only the remainder of it displaces the fluid in the upper layer. The fluid motion outside the plume and the fountain is upward in both layers, but with two different vertical velocities.

From our experimental observations, the steady state is attained after the fountain source injects 8 to 20 times as much fluid as the tank volume. Figure 4 shows the process of Experiment 5 reaching steady state. The evolution of the vertical reduced gravity distributions in the environment were measured from the start of the experiment to 100 min, at 10 min intervals. This experiment took about 100 min to reach steady state. The volume flux from the fountain nozzle was $13.8\,\text{cm}^3\,\text{s}^{-1}$ in tank 2, so the fountain source replenished the fluid in the tank about 8 times.

Figure 5 shows the profiles of another experiment, Experiment 7, approaching the steady state. The evolution of the vertical reduced gravity distributions in the environment were measured from the start of the experiment to 160 min, at 20 min intervals. This experiment took about 160 min to reach steady state.

Although Experiment 7 had the same supply volume flux and tank size as Experiment 5, the former took longer to reach steady state. The time for a system reaching steady state requires that both layers reach steady state. Since a lower buoyancy input in Experiment 7 induces a deeper upper layer, a fountain takes longer to replace the fluid in this deeper layer. Note that in both of these examples,
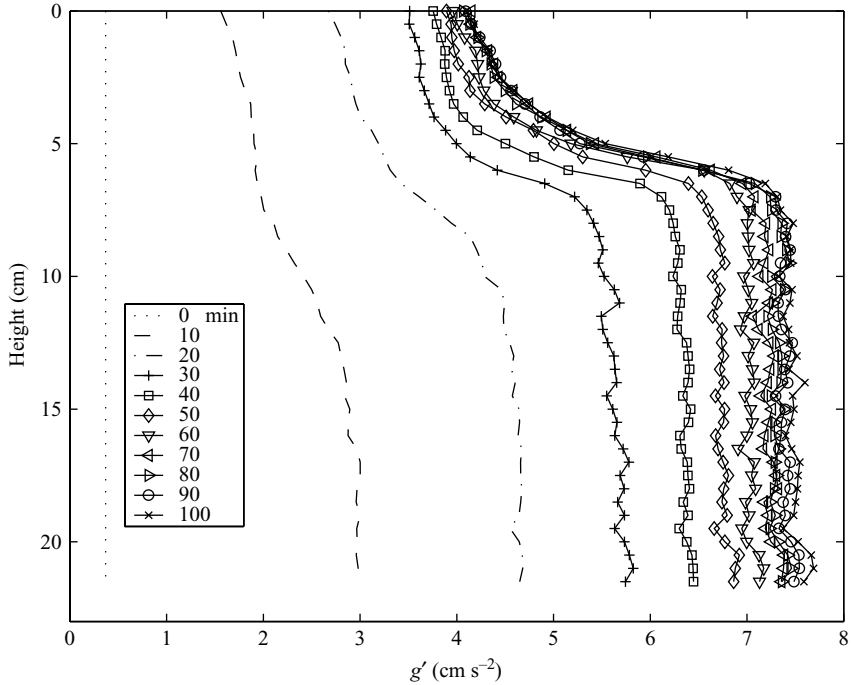
FIGURE 4. Transient reduced gravity profiles of Experiment 5 measured by the light attenuation technique. The profiles were measured from 0 to 100 min, at 10 min intervals, after turning on the plume and fountain sources. The upper layer has a weak vertical stratification and the lower layer is well-mixed in the transient state.
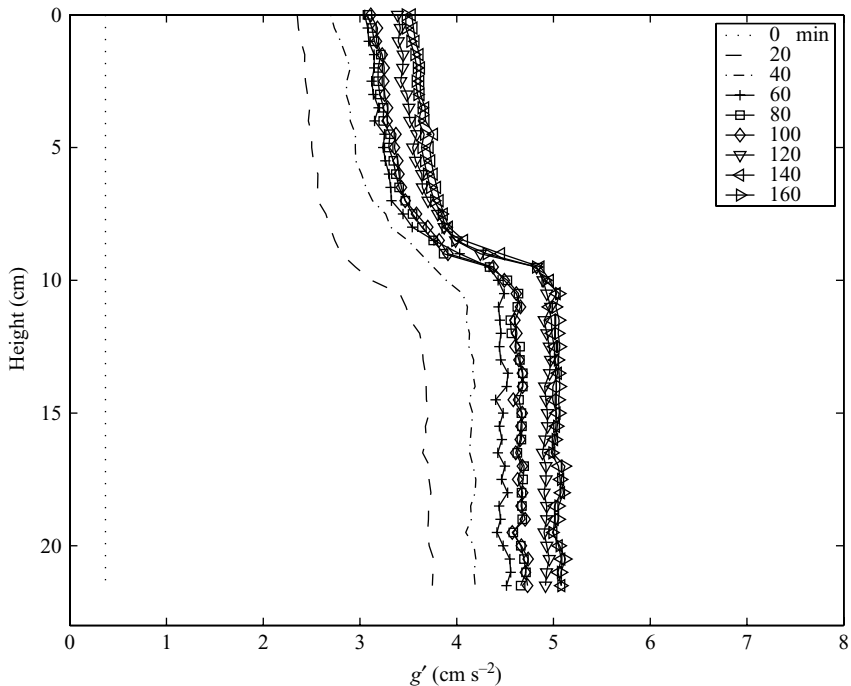

FIGURE 5. Transient reduced gravity profiles of Experiment 7 measured by the light attenuation technique. The profiles were measured from 0 to 160 min, at 20 min intervals, after turning on the plume and fountain sources.
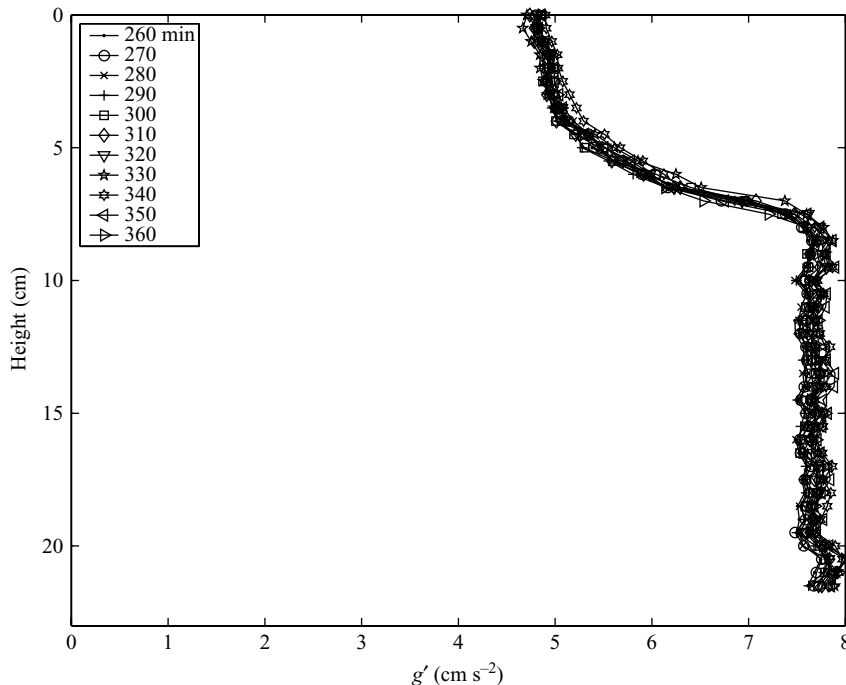
FIGURE 6. The reduced gravity profiles of the steady-state flow taken from Experiment 5. The profiles were measured after the experiment had run from 260 to 360 min, at 10 min intervals.

the shape of the profile is established relatively quickly and the densities of both layers simply increase until the steady state is reached.

4. Results

4.1. *Steady-state measurements*

A typical experiment reaches steady state between 1.5 and 3 h depending on the volume flux from the fountain and size of the tank. When the reduced gravity profiles varied less than $0.2 \, \mathrm{cm \, s^{-2}}$ and the interface depth difference was less than 0.5 cm (the spatial resolution of the profile) over 10 successive 1 min intervals, we deemed that the experiment had reached steady state. The reduced gravity value of $0.2 \, \mathrm{cm \, s^{-2}}$ was chosen as it corresponds to the experimental error in determining g'.

Figure 6 shows the reduced gravity profiles of the steady-state flow in Experiment 5 from 260 to 360 min, at 10 min intervals. The reduced gravity profiles fluctuate back and forth around the mean profile. Figure 7 shows the values of the reduced gravity in both layers, the reduced gravity step and the interface depth of Experiment 5 from the start of the experiment until it was ended. In this experiment, the upper-layer reduced gravity fluctuates back and forth around $4.7 \, \mathrm{cm \, s^{-2}}$ with a deviation amplitude $0.3 \, \mathrm{cm \, s^{-2}}$. The lower layer reduced gravity fluctuates back and forth around $7.3 \, \mathrm{cm \, s^{-2}}$ with a deviation amplitude of $0.4 \, \mathrm{cm \, s^{-2}}$. Both layers have similar deviations. The interface depth fluctuates around 7.5–8.5 cm with an average depth 7.8 cm. The reduced gravity step has a mean value $2.7 \, \mathrm{cm \, s^{-2}}$ with a deviation amplitude of about $0.2 \, \mathrm{cm \, s^{-2}}$. The deviations of measurements of the reduced gravity are within the experimental error and measured values of the interface depth have reasonable variations, less than 8%.
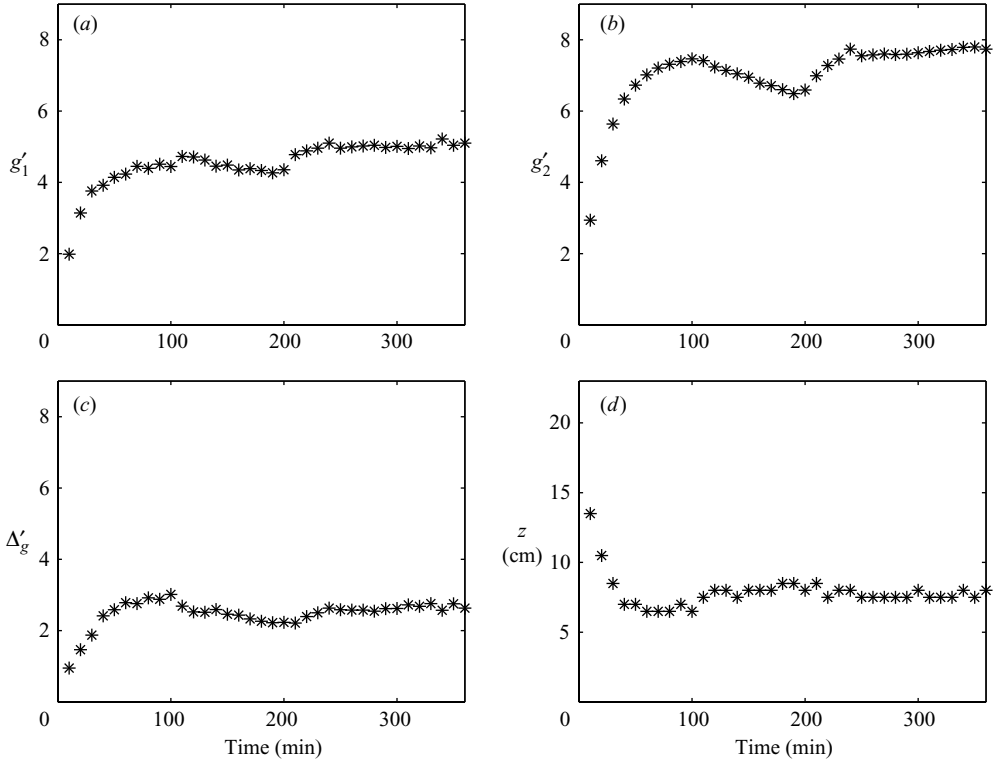
FIGURE 7. (*a*) and (*b*) present the values of the reduced gravity in both layers, (*c*) the reduced gravity step and (*d*) the interface depth in Experiment 5 as functions of time. Estimates of the entrainment rate E were made from 355 to 360 min, when the system appeared to be steady.

Figure 8 shows the reduced gravity profiles of the steady-state flow in Experiment 7 from 200 to 300 min, at 10 min intervals. Figure 9 shows the values of the reduced gravity in both layers, the reduced gravity step and the interface depth of Experiment 7. The upper layer reduced gravity fluctuates back and forth around $3.4 \, \mathrm{cm \, s^{-2}}$ with a deviation amplitude $0.3 \, \mathrm{cm \, s^{-2}}$ in the steady state. The lower-layer reduced gravity fluctuates back and forth around $4.7 \, \mathrm{cm \, s^{-2}}$ with a deviation amplitude $0.4 \, \mathrm{cm \, s^{-2}}$. The interface depth fluctuates around 9.5–$11.5 \, \mathrm{cm}$ with an average depth $10.4 \, \mathrm{cm}$. The reduced gravity step has a mean value $1.3 \, \mathrm{cm \, s^{-2}}$ with a deviation amplitude $0.2 \, \mathrm{cm \, s^{-2}}$. The deviations of the reduced gravity measurements are within the experimental error, but the interface depth measurements have larger variations, about 10%.

4.2. *Estimate of penetrative entrained volume flux*

The measurements of the reduced gravity g_1' and g_2' in the upper and lower layers, and the interface depth h are reported in table 2. The reduced gravity profiles of the last 6 min before the experiments terminated were used to estimate the penetrative entrained volume flux. The values in table 2 are the average values of those six consecutive profiles, and each two consecutive profiles have a 1 min interval. These values are obtained in the steady state, except for Experiment 1. Although Experiment 1 did not attain steady state, it achieved a quasi-steady state in which the values of reduced gravity and the interface depth changed gradually. We include this set of experimental results as it gives values consistent with the other experiments.
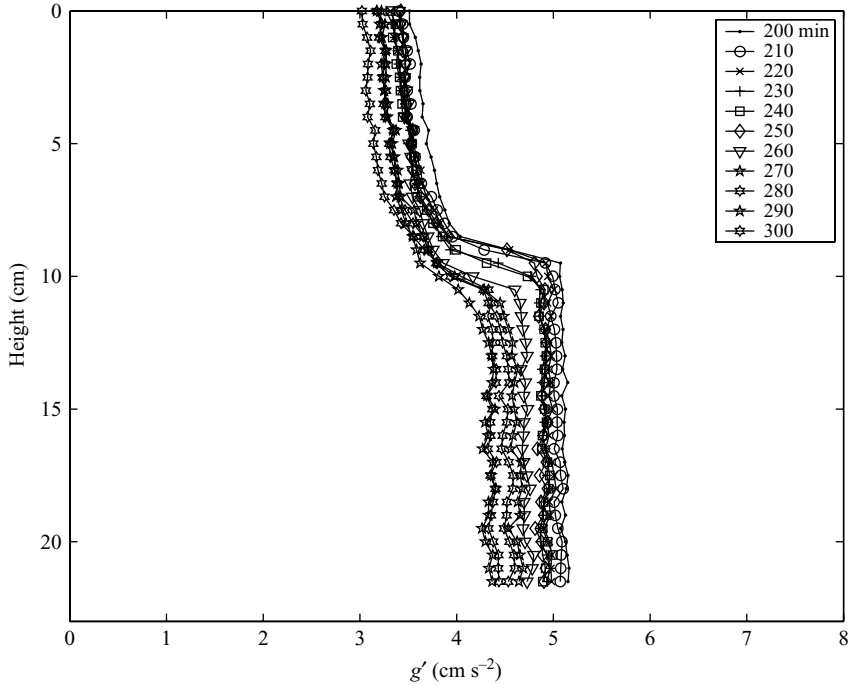
FIGURE 8. The reduced gravity profiles of the steady-state flow taken from Experiment 7. The profiles were measured after the experiment had run from 200 to 300 min, at 10 min intervals.

Run	g'_1	g'_2	h (cm)	Q_{E1} (cm^3 s^{-1})	Q_{E2} (cm^3 s^{-1})	Q_{E3} (cm^3 s^{-1})
1	3.1	5.6	7.6	21.3	18.4	25.4
2	3.5	4.9	15.3	65.7	60.7	64.5
3	3.5	5.7	8.4	21.9	22.2	20.8
4	2.9	3.8	15.5	55.5	60.7	45.6
5	5.0	7.7	7.9	23.0	27.0	26.6
6	3.7	4.8	13.0	48.8	67.7	60.5
7	3.1	4.3	10.5	30.5	35.8	35.0
8	2.4	3.2	14.4	49.2	75.0	60.4

TABLE 2. The experimental results of the reduced gravity values in the upper and lower layers, the interface depth and the penetrative entrained volume fluxes through the density interface in 8 different runs.

The estimates of the penetrative entrained volume fluxes Q_E by a turbulent fountain across the density interface are shown in table 2. Three different approaches to estimate the penetrative entrained volume flux have been described in §2.3, and now we discuss how these values are estimated from the experimental results.

Figure 10 shows the average reduced gravity profiles of the eight different experimental cases (as in table 1). From these profiles, the upper-layer reduced gravity g'_1 is then obtained by averaging the reduced gravity values above the interface and g'_2 by averaging the lower-layer reduced gravity. The interface position is selected where its reduced gravity difference with the upper-layer reduced gravity is 80% of
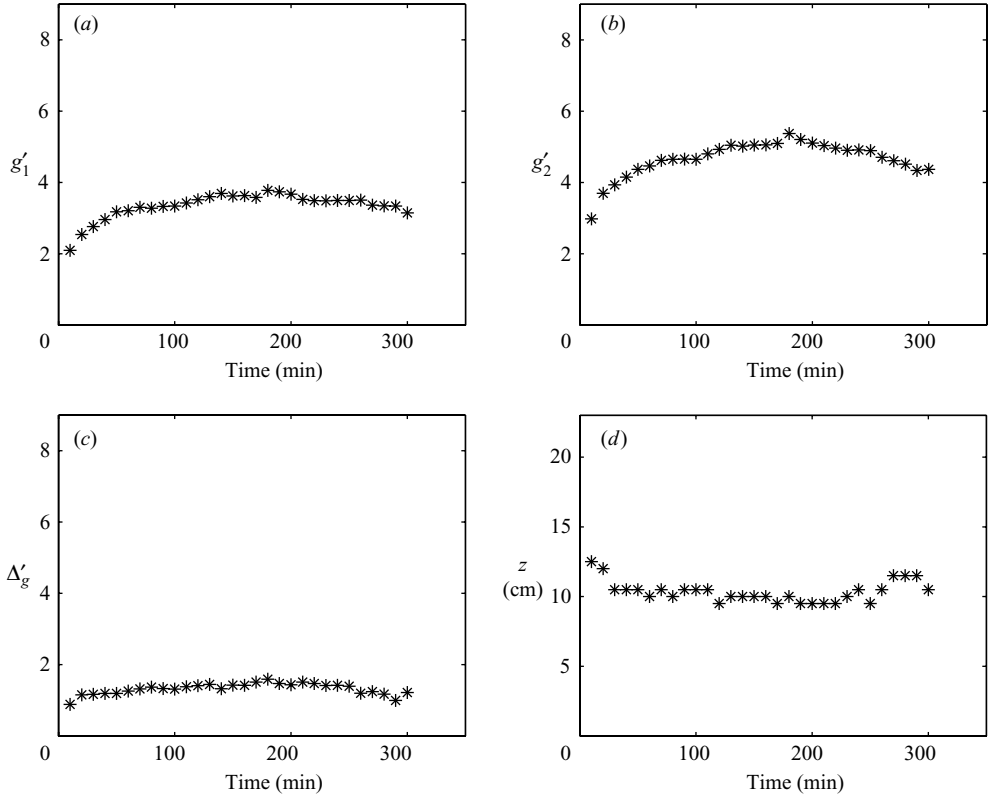
FIGURE 9. (*a*) and (*b*) present the values of the reduced gravity in both layers, (*c*) the reduced gravity step and (*d*) the interface depth in Experiment 7 as functions of time. Estimates of the entrainment rate E were made from 295 to 300 min, when the system appeared to attain steady.

the reduced gravity difference between the two layers, i.e.

$$h = z(g'_{int}) = z(g'_1 + 0.8\Delta g'), \tag{4.1}$$

where $\Delta g' = g'_2 - g'_1$.

In experiments there is no clear-cut interface, but rather there is an intermediate region having a strong gradient and ranging in thickness from 2 to 3 cm. The interface position was selected as close as possible to the depth where the value of lower-layer reduced gravity was attained, since theoretically we expect a uniform lower-layer reduced gravity in the steady state, as observed in the experimental results.

Theoretically, the reduced gravity of the lower layer is identical to the reduced gravity of the plume at the interface, that is, the interface is where the plume has the lower-layer reduced gravity. In the experimental data, 80% of the reduced gravity difference from the upper-layer reduced gravity is chosen as the interface reduced gravity rather than the lower-layer reduced gravity value since using the average lower-layer reduced gravity sometimes over-estimates the interface position. However, the difference between these two positions is less than 0.5 cm from our experimental observations.

As an example, figure 11 shows the measured average reduced gravity profile of Experiment 7 along with the estimated values of the upper-layer, lower-layer reduced
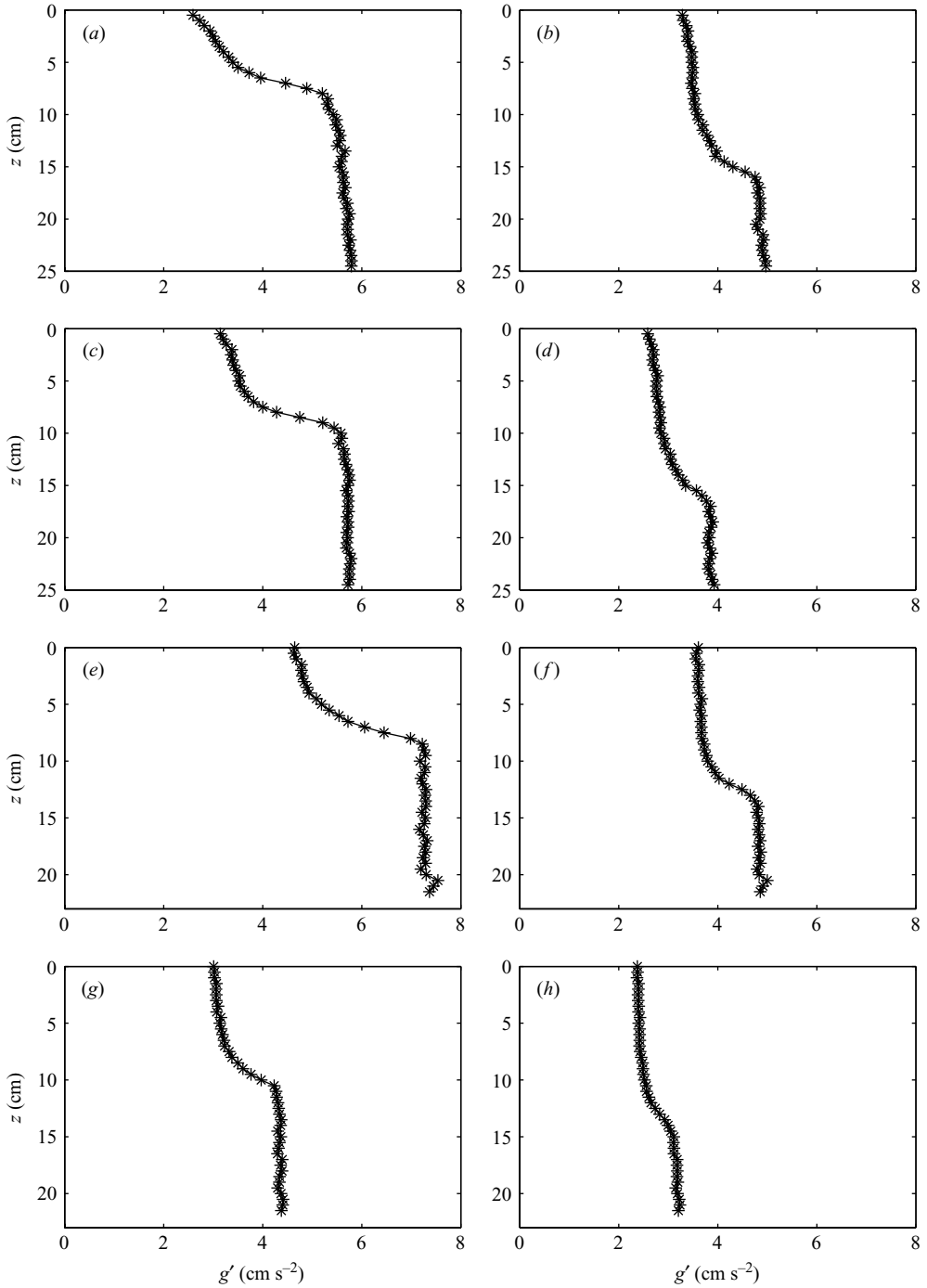
FIGURE 10. The average reduced gravity profiles of 8 experimental cases whose environmental conditions are presented in table 1.

gravity and the interface depth determined from this profile. A uniform upper-layer reduced gravity is not as clear as that in the lower layer, and a slight stable stratification forms in this layer. In our analysis, we used the average reduced gravity
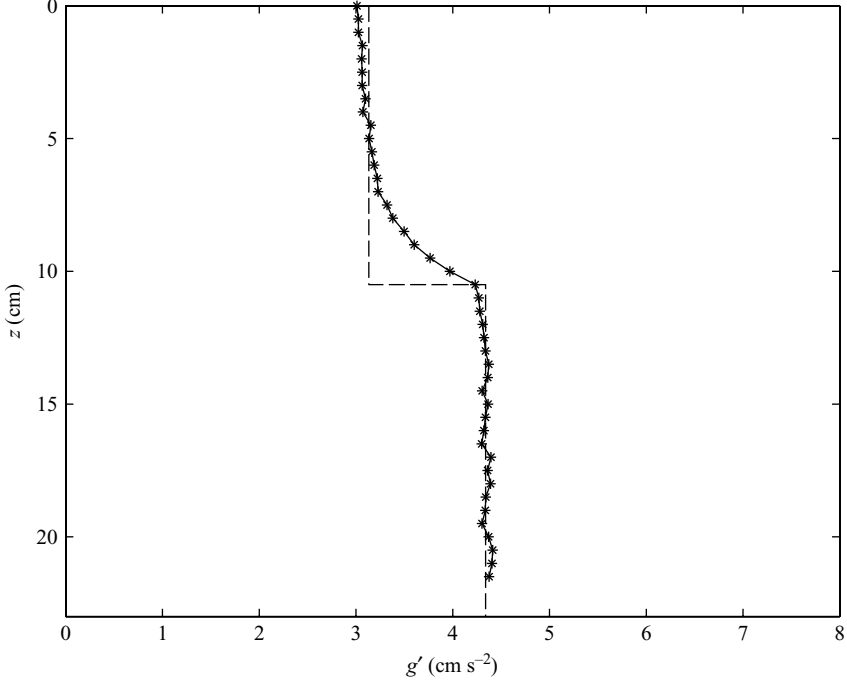
FIGURE 11. Experimental measured reduced gravity values in Experiment 7 (∗ marks) along with the estimated reduced gravity values (dashed line) in two layers and the estimated interface position.

value of the upper layer, and the deviation between the average reduced gravity and the upper-layer reduced gravity is less than $0.3 \, \mathrm{cm \, s^{-2}}$.

Three different measurements of the penetrative entrained volume flux Q_E are obtained from (2.8) and the plume theory (2.9a) (denoted as Q_{E1})

$$Q_{E1} = Q_p = C B_r^{1/3} h^{5/3}, \tag{4.2}$$

from the fountain volume flux using (2.12) (denoted as Q_{E2})

$$Q_{E2} = \frac{g_1' Q_f}{\Delta g'} \tag{4.3}$$

and from measurements of the reduced gravity of the layers and the buoyancy flux from the plume using (2.18) (denoted as Q_{E3})

$$Q_{E3} = \frac{B}{\Delta g'}. \tag{4.4}$$

In order to use plume theory to measure Q_{E1}, it is necessary to determine the virtual origin. The equations to calculate the virtual original height z_v in this study are given by Hunt & Kaye (2001). The virtual origin heights were calculated to be $z_v = 1.2 \sim 1.4 \, \mathrm{cm}$ depending on different plume source conditions. From the plume equation (2.9) and the virtual original height, the volume flux Q_p in the plume at the density interface is expressed as

$$Q_{E1} = Q_p = C B_r^{1/3} (h + z_v)^{5/3}. \tag{4.5}$$

Q_{E1} was used as a reference value for comparing deviations between the measured penetrative entrained volume fluxes. The variations between the values estimated by these three methods are within 50%, but most data are within 20%.

Theoretical estimated values of Q_{E1} have a high sensitivity on the values of the estimated interface position since the volume flux depends on $h^{5/3}$. Consequently, the determination of the interface depth is important for the penetrative entrainment values determined by this method. The values Q_{E2} and Q_{E3}, determined from (2.12) and (2.18), are sensitive to the values of the reduced gravity step between two layers, especially when the reduced gravity step is small. Supposing an inherent experimental measurement error on determination of the reduced gravity step by the lighting intensity attenuation technique is ($\Delta g'_{err} = 0.2\,\text{cm}\,\text{s}^{-2}$), the large reduced gravity step in Experiments 1 ($2.5\,\text{cm}\,\text{s}^{-2}$) or 5 ($2.4\,\text{cm}\,\text{s}^{-2}$) does not have such a large error as the small reduced gravity step in Experiments 4 ($0.9\,\text{cm}\,\text{s}^{-2}$) or 8 ($0.8\,\text{cm}\,\text{s}^{-2}$). The former cases may result in $8 \sim 9\%$ error since the inherent measurement error is small compared to the reduced gravity step value, but the latter ones result in a larger error of about $25 \sim 30\%$.

4.3. *Estimate of penetrative entrainment rate*

The fountain model proposed by Bloomfield & Kerr (2000) is applied here to estimate the values of the radius b_{int}, the vertical velocity w_{int} and the volume flux Q_{int} in the fountain at the density interface before the fountain reverses at its maximum depth. The fountain model is used here without considering the reversal of the fountain which changes some dynamical properties in the fountain. The opposite direction momentum of the outer annular jet modifies the momentum of the inner core jet after the reversal. The discussion on this phenomena was presented in Turner (1966) and Bloomfield & Kerr (2000). In the present experiments, the outer annular jet does not enclose the core jet over its full depth since the fluid in the outer annular jet spreads laterally after it rises back to the upper layer. The entrained fluid by the turbulent fountain is heavier than the fluid in the upper layer. Therefore, the influence of the outer annular jet on the core jet in this experimental apparatus is not as significant as that in a normal fountain structure.

The fountain model which was used to estimate the local values at the interface in the fountain has a Gaussian entrainment constant proposed by Bloomfield & Kerr (2000) $\alpha_g = 0.06$ ($0.06 \times \sqrt{2}$ for the top-hat distribution), which lies between the plume value 0.083 (Turner 1986) and the jet value 0.054 (Albertson *et al.* 1950). The initial conditions, the volume flux Q_f and the momentum flux M_f from the fountain nozzle, and the environmental conditions, the reduced gravity in two layers, were applied in the calculations.

Table 3 shows the local Richardson number values, the velocity, the radius and the volume flux at the density interface obtained from the numerical calculations of the fountain model, and the penetrative entrainment rates E at the density interface by three different methods. The penetrative entrainment rate $E_1 = Q_{E1}/Q_{int}$, which is estimated by the plume theory and the fountain model, results in the smallest variations in these three approaches, while $E_2 = Q_{E2}/Q_{int}$ and $E_3 = Q_{E3}/Q_{int}$ have similar amounts of variability.

In these experiments, the local Richardson numbers are small, $Ri < 1.2$, at the density interface. In this range of Richardson numbers, an approximately constant value 0.65 (± 0.17) of the penetrative entrainment rate was observed in our experimental data of both steady state and quasi-steady state. Figure 12 shows plots of the penetrative entrainment rates from the three independent estimates against

Run	Ri	Q_{int} (cm^3 s^{-1})	w_{int} (cm s^{-1})	b_{int} (cm)	E_1	E_2	E_3
1	0.49	37.0	3.1	1.9	0.58	0.50	0.69
2	0.70	93.7	2.6	3.4	0.70	0.65	0.69
3	0.72	39.0	2.6	2.2	0.56	0.57	0.53
4	0.38	95.7	2.8	3.3	0.58	0.63	0.48
5	1.17	36.8	2.2	2.3	0.63	0.73	0.72
6	0.29	83.9	3.3	2.9	0.58	0.81	0.72
7	0.90	44.4	1.9	2.7	0.69	0.81	0.79
8	0.22	91.5	3.3	3.0	0.54	0.82	0.66

TABLE 3. The local values of the Richardson number, the impinging volume flux, the vertical velocity and the radius at the density interface estimated by the fountain model. The penetrative entrainment ratios by three different estimation approaches are shown as well.
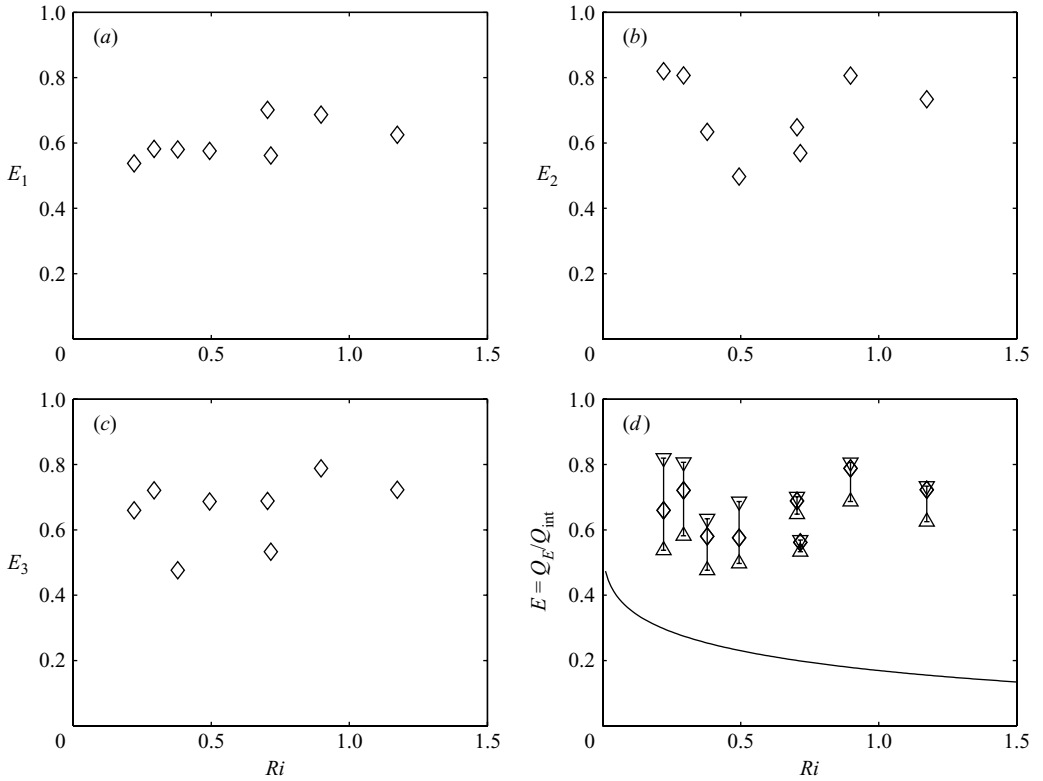

FIGURE 12. The penetrative entrainment rate E_1, E_2 and E_3 by three estimation approaches against Richardson number are presented in (*a*), (*b*) and (*c*). (*d*) The scatter range of the penetrative entrainment rate between these three approaches against the Richardson number and the solid line is calculated from (1.5) from penetrative entrainment of a buoyant plume by Kumagai (1984).

the Richardson number. The penetrative entrainment rate scatters around $E = 0.65$ in each case. The penetrative entrainment rate E_1 has the smallest scatter (standard deviation $= 0.06$). The penetrative entrainment rates E_2 and E_3 have similar standard deviation values of 0.12 and 0.10, respectively. The data shown in figure 12 are the entrainment rates determined by the three methods, and the error has reflected the

total scatter in the values. The solid line in figure 12(*d*) is obtained from (1.5) which presents the penetrative entrainment rate of a buoyant plume during the same range of Richardson numbers by Kumagai (1984). The results of Baines, Corriveau & Reedman (1993) show a larger scatters of entrainment rate, but they are in a similar scale to our results (see figure 6 of their paper.)

5. Discussion

5.1. *Characteristics of the flow*

The fluid in the lower layer is supplied by the plume and withdrawn by the penetrative entrainment of the fountain. The two interface fluxes have to balance in the steady state. The supply fluid from the plume spreads out as a layer at the bottom of the tank and the penetrative entrainment by a fountain entrains a certain amount of dense fluid in the lower layer into the upper layer. The fluid in the upper layer is supplied by the reversal of the fountain at the base of the layer, and removed by the siphon pipe at the top of the tank and also by entrainment into the plume. The sum of the latter two elements balances the supply in this layer in the steady state.

The fluid in the upper layer is supplied by the penetrative entrainment of the fountain at the bottom of the layer. A uniform upper-layer reduced gravity is not observed as clearly as that in the lower layer; instead the experiments show that a slight stable stratification forms in this layer. The cause of this stable stratification is probably the turbulent fluctuations at the density interface. If the reduced gravity of the lower layer is constant and the fountain entrains at a constant rate, the supply fluid to the upper layer should have a constant reduced gravity. However, if the penetrative entrained volume flux at the density interface has fluctuations, the reduced gravity of the fluid entering the upper layer will vary, leading to a stable stratification in the upper layer.

Different properties from the plume and fountain sources produce different flow patterns. A large source volume flux Q_f from the fountain source induces a small reduced gravity in the upper layer in the steady state when the other conditions are fixed. A large buoyancy flux B from the plume source produces high reduced gravity values in both layers. Increasing the momentum flux M_f from the fountain source increases the interface depth and decreases the buoyancy contrast across the interface.

The buoyancy flux of the plume source and the penetrative entrained volume flux at the density interface by the fountain determine the magnitude of the reduced gravity step. A larger penetrative entrained volume flux across a density interface induces a smaller reduced gravity step. When the penetrative entrained volume flux is infinitely large, there is no density interface and the entire space is well mixed. Hence, if a fountain is supplied by a very high momentum flux, this momentum promotes complete mixing in the space (Hunt, Cooper & Linden 2000).

5.2. *Plume theory*

Plume theory (2.9*b*) can be applied to calculate the reduced gravity step between two layers as

$$\Delta g'_p = \Delta g'(h, B_r) = \frac{1}{C} B_r^{2/3} (h + z_v)^{-5/3}, \tag{5.1}$$

in order to compare the differences between the theoretical estimations and the experimental measurements. The values of the reduced gravity step determined from

Run	$\Delta g'_p$ (cm s^{-2})	$\Delta g'_{pe}$ (cm s^{-2})	g'_{1c} (cm s^{-2})	g'_1 (cm s^{-2})
1	3.0	2.5	5.7	3.1
2	1.3	1.4	3.8	3.5
3	2.1	2.2	3.3	3.5
4	0.8	0.9	2.2	2.9
5	2.8	2.7	5.7	5.0
6	1.5	1.1	3.7	3.7
7	1.4	1.2	3.1	3.1
8	0.9	0.8	2.0	2.4

TABLE 4. Two sets of values of the reduced gravity step values at the density interface and the reduced gravity values that the upper layer should attain in the steady state. The reduced gravity step values at the density interface by the plume theory and the experimental measurements are also given. The estimated reduced gravity values that the upper layer should attain in the steady state with the measured values in the laboratory are presented to see the differences between them.

experimental results are obtained by

$$\Delta g'_{pe} = g'_2 - g'_1, \tag{5.2}$$

where g'_1 and g'_2 are the average measured values in table 2.

Table 4 presents these two sets of the reduced gravity step at the density interface ($\Delta g'_p$ and $\Delta g'_{pe}$). In general, the values of the reduced gravity step between the density interface calculated by the plume theory are in good agreement with the experimental results. The maximum difference in these experiments is 0.5 cm s^{-2}, and most of experimental results are within 0.2 cm s^{-2}.

Table 4 also shows the estimated reduced gravity values g'_{1c}, which the upper layer should attain in the steady state (see (2.4) and here the small volume flux from the plume source Q_s is retained to obtain a more accurate value),

$$g'_{1c} = \frac{B}{Q_{out}} = \frac{B}{Q_f + Q_s}, \tag{5.3}$$

and experimental measured values g'_1 in the upper layer. Obviously, Experiment 1 did not achieve a steady state. The rest of the experimental data and theoretical values agree to within 0.7 cm s^{-2} (Experiment 4) and most of the data are within 0.3 cm s^{-2}.

5.3. *Fountain model*

The magnitudes of the final depth which a turbulent fountain is able to reach in the steady state, z_{mc} estimated by the fountain model of Bloomfield & Kerr (2000) and z_{me} observed from the experiments, are given in table 5. The numerically calculated values of the final depth are where the downward momentum is reduced to zero. The experimental values are determined from the images such as those in figure 13. Comparing the intensity variations below the fountain source nozzle, we take the final depth as the maximum distance below the fountain source at which fountain fluid appears.

The vertical penetrative depth h_d ($=z_{me} - h$) of a turbulent fountain into the lower layer was observed to be proportional to the local radius b_{int} of the fountain at the density interface (cf. figure 13). This feature was consistent in all of our experiments. This self-similar shape of penetration by a turbulent fountain is similar to that by a buoyant plume reported by Baines (1975).

Run	z_{mc} (cm)	z_{me} (cm)
1	11.3	10.4
2	20.3	21.3
3	11.2	11.3
4	22.7	21.8
5	9.4	11.0
6	19.7	18.1
7	12.7	14.1
8	24.4	20.1

TABLE 5. The final depths of the fountain are determined from the numerical fountain model z_{mc} and observed in the experiments z_{me}.
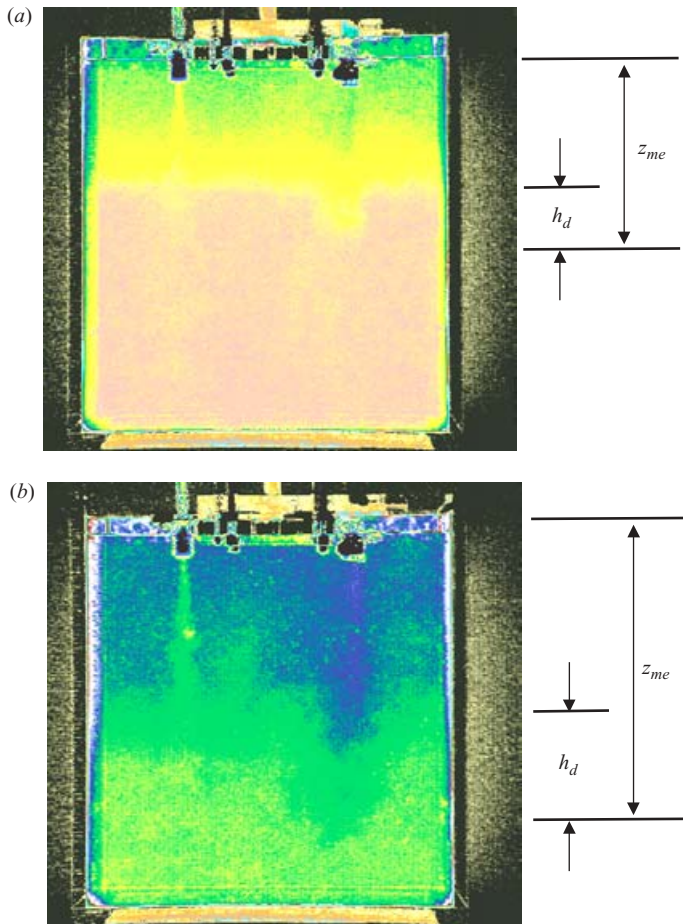
COLOUR

FIGURE 13. The vertical penetrative depth h_d into the dense lower layer by a fountain is roughly proportional to the radius b_{int} of the fountain at the density interface. (*a*) The initial momentum of the fountain is small, the penetrative depth is short and so is the radius of the fountain at the interface. The image was taken in the steady state of Experiment 5. (*b*) The initial momentum of the fountain is large, the penetrative depth is long and so is the radius of the fountain at the interface. The image was taken in the steady state of Experiment 6.

Shy (1995), from his experimental data, showed the relationship between the dimensionless penetration depth ($P_d = h_d/2b_{int}$) and the Richardson number as

$$P_d = K \, Ri^{-1}, \tag{5.4}$$

where $K = 0.72$ is an experimentally determined constant. This relationship is not observed in our experimental results, maybe because the Richardson numbers in our experiments are all smaller than 1.2. However, our results are consistent with the maximum value of P_d, about 1, reported in Shy (1995).

The fountain model is adopted to estimate the physical parameters in the fountain at the density interface. The source conditions of the fountain given in table 1 are applied in our numerical calculations. This model has a reasonable agreement with the experimental results on the final depth that a fountain is able to reach (see table 5).

5.4. *Penetrative entrainment at small Richardson numbers*

At small Richardson numbers, the entrainment is quantitatively different from that at large Richardson numbers, since the effect of the density step at the interface is small. The fountain reverses owing to its negative buoyancy, not owing to the impact on the interface. Kumagai (1984) presented limited experimental data in the range of small Richardson numbers, $Ri < 1.2$. The range of Richardson numbers is from 0.1 to 70 in his experimental data, but most of them are larger than 1.2.

Kumagai (1984) claimed to observe a constant penetrative entrainment rate when Richardson numbers were small ($Ri < 0.25$, see figure 12 in his paper). The value ($E = 0.32$) he reported from his experimental results is smaller than the results obtained in this study. However, that asymptotic constant ($E = 0.56$) from his empirical equation ((1.5)) is contained in our experimental results (0.65 ± 0.17).

From our experimental results at small Richardson numbers, the penetrative entrainment scales with two parameters, the contact area (A_{int}) and the vertical velocity (w_{int}) in the turbulent fountain at the interface. The large contact area increases the area of mixing with the lower layer. The large impinging velocity induces more entrainment into the turbulent fountain in the heavy layer and causes a greater penetration depth across the interface. Both parameters increase the amount of penetrative entrainment into the fountain from the heavy layer to the light layer. The product of these two parameters is the impinging volume flux at the density interface, which is considered as the parameter related to the penetrative entrainment by a turbulent fountain at small Richardson number.

6. Conclusions

In this paper, we investigated the penetrative entrainment across a density interface between two layers by a turbulent fountain. A new experimental arrangement was set up to measure the penetrative entrainment by a turbulent fountain and the steady-state flow was analysed. A theoretical model was established by assuming that the stratification consists of two uniform layers. Experiments were conducted in two different Plexiglas tanks, using salt solution and water as working fluids. Experimental results were described qualitatively and presented quantitatively. Quantitative values of the penetrative entrainment rate were determined.

The penetrative entrainment by a turbulent fountain is estimated quantitatively by three independent formulae. These formulae are based on the penetrative entrainment volume flux equal to the supply volume flux in the plume, the penetrative entrainment

by the fountain across the density interface and the entrainment by the plume within the upper layer.

From experimental observation, the time to reach the steady state in the environment depends on the volume flux from the fountain source and the tank size. The time to replace the lower-layer fluid depends on the size of the lower-layer and the penetrative entrained volume flux at the interface. The time to replace the upper-layer fluid depends on the size of the upper layer and the volume flux from the fountain source.

Two quasi-uniform layers in the steady state were observed in the laboratory experiments. The reduced gravity profile in the steady state has small fluctuations around the mean profile. The lower layer has a nearly uniform reduced gravity value, but there is a slight stable stratification in the upper layer. The stable stratification in the upper layer may be caused by fluctuations of the turbulent fountain at the density interface.

The penetrative entrained volume fluxes are determined from experimental data. Three independent estimates have a maximum deviation of 50% between them, and most are within 20%. Plume theory is applied to estimate the volume flux and the reduced gravity in the plume and it shows good agreement with experimental results of the measured reduced gravity values which are determined by the lighting attenuation technique. The penetrative entrained volume flux Q_{E1} is estimated from the plume theory. The penetrative volume fluxes Q_{E2} and Q_{E3} are sensitive to the accuracy of the measured reduced gravity. When the reduced gravity step between two layers is smaller, the measurement accuracy is more sensitive to estimates of the penetrative entrained volume fluxes. The three calculation methods give results in reasonable agreement with each other.

The fountain model is used to estimate the values of the volume flux, the velocity and the radius in the turbulent fountain. The penetrative entrainment rate E is defined as the volume flux entrained by the fountain normalized by the volume flux in the fountain at the interface. The value E_1, which is estimated by the plume theory and the fountain model, results in the smallest scatter between three penetrative entrainment rates. The penetrative entrainment rates E_2 and E_3, which are estimated by the measured reduced gravity, the volume flux of the fountain source and the buoyancy flux of the plume respectively, have a similar scatter.

Our experimental results show a nearly constant penetrative entrainment rate ($E = 0.65 \pm 0.17$) by a turbulent fountain at small local Richardson number. The local Richardson numbers are smaller than 1.2 in all of the experiments presented in this study. This nearly constant penetrative entrainment rate by a turbulent fountain is larger than those reported previously for a plume and this difference may be a result of differences in their internal structures.

REFERENCES

ALBERTSON, M. L., DAI, Y. B., JENSEN, R. A. & ROUSE, H. 1950 Diffusion of submerged jets. *Trans. ASCE* **115**, 639–697.

BAINES, W. D. 1975 Entrainment by a plume or jet at a density interface. *J. Fluid Mech.* **68**, 309–320.

BAINES, W. D., CORRIVEAU, A. F. & REEDMAN, T. J. 1993 Turbulent fountains in a closed-chamber. *J. Fluid Mech.* **255**, 621–646.

BAINES, W. D., TURNER, J. S. & CAMPBELL, I. H. 1990 Turbulent fountains in an open chamber. *J. Fluid Mech.* **212**, 557–592.

BAUMAN, F. S. 2003 *Underfloor Air Distribution (UFAD) Design Guide*. American Society of Heating, Refrigerating and Air-Conditioning Engineers. ISBN 1-931862-21-4.

BLOOMFIELD, L. J. & KERR, R. C. 1998 Turbulent fountains in a stratified fluid. *J. Fluid Mech.* **358**, 335–356.

BLOOMFIELD, L. J. & KERR, R. C. 2000 A theoretical model of a turbulent fountain. *J. Fluid Mech.* **424**, 197–216.

CARDOSO, S. S. S. & WOODS, A. W. 1993 Mixing by a turbulent plume in a confined stratified region. *J. Fluid Mech.* **250**, 277–305.

CENEDESE, C. & DALZIEL, S. B. 1998 Concentration and depth fields determined by the light transmitted through a dyed solution. In *Proc. 8th Intl Symp. on Flow Visualization* (ed. G. M. Carlomagno & I. Grant), paper 061 ISBN 0953399109.

HUNT, G. R., COOPER, P. & LINDEN, P. F. 2000 Thermal stratification caused by plumes and jets in enclosed spaces. In *Proc. Roomvent 2000 7th Intl Conf. on Air Distribution in Rooms* (ed. H. B. Awbi), pp. 191–198. Reading, UK. Elsevier Science, ISBN 0-080-43017-1.

HUNT, G. R. & KAYE, N. G. 2001 Virtual origin correction for lazy turbulent plumes. *J. Fluid Mech.* **435**, 377–396.

HUNT, G. R. & LINDEN, P. F. 2001 Steady-state flows in an enclosure ventilated by buoyancy forces assisted by wind. *J. Fluid Mech.* **426**, 355–386.

KUMAGAI, M. 1984 Turbulent buoyant convection from a source in a confined two-layered region. *J. Fluid Mech.* **147**, 105–131.

LARSON, M. & JONSSON, L. 1994 Mixing in a 2-layer stably stratified fluid by a turbulent jet. *J. Hydraul. Res.* **32** (2).

LARSON, M. & JONSSON, L. 1996 Efficiency of mixing by a turbulent jet in a stably stratified fluid. *Dyn. Atmos. Oceans* **24**, 63–74.

LIN, Y. J. P. & LINDEN, P. F. 2002 Buoyancy-driven ventilation between two chambers. *J. Fluid Mech.* **463**, 293–312.

LIN, Y. J. P. & LINDEN, P. F. 2005 The model of under floor air distribution systems. *Energy Build.* **37**, 399–409.

LINDEN, P. 1973 The interaction of a vortex ring with a sharp density interface: a model for turbulent entrainment. *J. Fluid Mech.* **60**, 467–480.

MCDOUGALL, T. J. 1981 Negatively buoyant vertical jets. *Tellus* **33**, 313–320.

MIZUSHINA, T., OGINO, F., TAKEUCHI, H. & IKAWA, H. 1982 An experimental study of vertical turbulent jet with negative buoyancy. *Warme and Stoffubertragung* (*Thermo and Fluid Dynamics*) **16**, 15–21.

MORTON, B. R. 1959 Forced plumes. *J. Fluid Mech.* **5**, 151–163.

MORTON, B. R. 1962 Coaxial turbulent jets. *Intl J. Heat Mass Transfer* **5**, 955–965.

MORTON, B. R., TAYLOR, G. I. & TURNER, J. S. 1956 Turbulent gravitational convection from maintained and instantaneous sources. *Proc. R. Soc. Lond.* A **234**, 1–23.

SHY, S. S. 1995 Mixing dynamics of jet interaction with a sharp density interface. *Expl Therm. Fluid Sci.* **10**, 335–369.

STEPHENS, R. & IMBERGER, J. 1993 Reservoir destratification via mechanical mixers. *J. Hydraul. Engng ASCE* **119**, 438–457.

TURNER, J. S. 1966 Jets and plumes with negative or reversing buoyancy. *J. Fluid Mech.* **26**, 779–792.

TURNER, J. S. 1968 The influence of molecular diffusivity on turbulent entrainment across a density interface. *J. Fluid Mech.* **33**, 639–656.

TURNER, J. S. 1986 Turbulent entrainment: the development of the entrainment assumption. *J. Fluid Mech.* **173**, 431–472.

WEBSTER, T., BAUMAN, F. & REESE, J. 2002 Underfloor air distribution: thermal stratification. *ASHRAE J.* **44**, 28–36.